JACS
JOURNAL OF THE AMERICAN CHEMICAL SOCIETY

Article

pubs.acs.org/JACS

Two-Dimensional Charge Disproportionation of the Unusual High Valence State Fe^{4+} in a Layered Double Perovskite

Yoshiteru Hosaka,[†] Noriya Ichikawa,[†] Takashi Saito,[†] Pascal Manuel,[‡] Dmitry Khalyavin,[‡] J. Paul Attfield,[§] and Yuichi Shimakawa*[,†,∥]

[†]Institute for Chemical Research, Kyoto University, Uji, Kyoto 611-0011, Japan

[‡]ISIS, Rutherford Appleton Laboratory, Harwell Oxford, Didcot OX11 0QX, United Kingdom

[§]Centre for Science at Extreme Conditions and School of Chemistry, University of Edinburgh, Mayfield Road, Edinburgh EH9 3JZ, United Kingdom

[∥]Japan Science and Technology Agency, CREST, Uji, Kyoto 611-0011, Japan

Supporting Information

ABSTRACT: The crystal and magnetic structures of charge-disproportionated Ca_2FeMnO_6 were analyzed by neutron powder diffraction. Ca_2FeMnO_6 is a layered double perovskite oxide with a two-dimensional arrangement of Mn^{4+} and unusual high valence Fe^{4+} at room temperature. When cooled, the compound shows charge disproportionation followed by magnetic transition. Around 200 K, the Fe^{4+} shows the charge disproportionation to Fe^{3+} and Fe^{5+}, which are ordered in a checkerboard pattern in the two-dimensional FeO_6 octahedral layers. The magnetic transition occurs at 95 K, which is much lower than the charge disproportionation temperature. The magnetic structure is commensurate but noncollinear, and the antiferromagnetic coupling of Fe^{3+} and Fe^{5+} spins in the FeO_6 octahedral layers gives the ferrimagnetic moments. The unique magnetic structure is described as a result of two-dimensional localization of the ligand holes with effective spins.

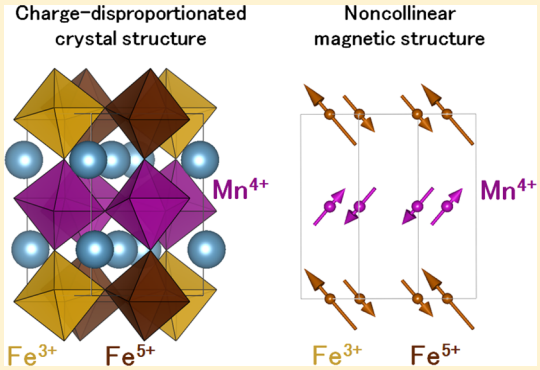

INTRODUCTION

Many iron oxides contain Fe^{2+} and/or Fe^{3+} because these oxidation states are very stable in octahedral and tetrahedral oxygen coordinations. In the simple perovskite $AFe^{4+}O_3$ (A = Ca^{2+}, Sr^{2+}, Ba^{2+}) synthesized under strongly oxidizing conditions, however, unusual high oxidation states of Fe like Fe^{4+} can be stabilized.[1−3] Since the energy levels of the 3d orbitals in Fe^{4+} are rather low because of the reduced screening effect of the core electrons, the low-lying Fe-3d orbitals strongly hybridize with O-2p orbitals, and as a result, oxygen p holes (ligand holes, $\underline{L}$) are produced in the electronic structure of the perovskites.[4,5] These ligand holes are the reason that Fe^{4+}, which is expected to have $t_{2g}^3e_g^1$ electron configuration, does not induce Jahn−Teller distortion like the isoelectronic Mn^{3+} does. The ligand holes are mobile at high temperatures, leading to metallic conduction, but they often become unstable at low temperatures.[6,7] The instability of the high oxidation state of Fe^{4+} is relieved by charge disproportionation (CD) from Fe^{4+} to Fe^{3+} and Fe^{5+}. In the ground state, the ligand holes are localized alternately at the Fe sites, and the CD transition ($2Fe^{4+} \rightarrow Fe^{3+} + Fe^{5+}$) can be described as $2d^5\underline{L} \rightarrow d^5 + d^5\underline{L}^2$.

$CaFeO_3$ shows this CD at 290 K, and the transition is accompanied by a metal-to-insulator transition and an orthorhombic-to-monoclinic structural transition.[6−9] The narrow conduction bands in $CaFeO_3$ with a distorted perovskite structure, unlike the wide conduction bands in cubic $SrFeO_3$, enhance the instability of ligand holes. Below the CD transition temperature, the charge-disproportionated Fe^{3+} and Fe^{5+} ions at the B sites in the perovskite structure are ordered in a rock-salt manner.[10,11] Magnetic transition is induced in the charge-disproportionated $CaFe^{3+}_{0.5}Fe^{5+}_{0.5}O_3$. Competing antiferromagnetic and ferromagnetic interactions between the Fe spins in charge-disproportionated $CaFe^{3+}_{0.5}Fe^{5+}_{0.5}O_3$ stabilize a helical magnetic structure below a magnetic transition at 115 K.[10] A similar CD transition at 210 K is observed in an A-site-ordered double perovskite $CaCu_3Fe_4O_{12}$ with Fe^{4+}.[12,13] At the CD transition, $CaCu_3Fe_4O_{12}$ shows a metal-to-semiconductor transition and a cubic ($Im\bar{3}$)-to-cubic ($Pn\bar{3}$) structural transition. The charge-disproportionated Fe^{3+} and Fe^{5+} ions at the B sites are similarly ordered in a rock-salt manner in the $Pn\bar{3}$ cubic lattice below the transition temperature. Interestingly, in $CaCu_3Fe_4O_{12}$, the magnetic transition occurs simultaneously with the CD transition. Both charge-disproportionated B-site Fe^{3+} and Fe^{5+} spins couple antiferromagnetically with the A'-site Cu^{2+} spins, leading to a ferrimagnetism with large magnetization (9.7 μ_B/f.u.).[14,15]

Received: April 9, 2015
Published: May 27, 2015

DOI: 10.1021/jacs.5b03712
J. Am. Chem. Soc. 2015, 137, 7468−7473

A new compound containing the unusual high valence state Fe^{4+} was recently obtained by low-temperature topochemical oxidation of the brownmillerite Ca_2FeMnO_5.[16,17] The compound is a fully oxygenated double perovskite Ca_2FeMnO_6 with a layered arrangement of $Fe^{4+}O_6$ and $Mn^{4+}O_6$ octahedra (Figure 1) and is the first compound that has an isolated two-dimensional layered arrangement of high valent Fe^{4+}. The crystal structure at room temperature has a $2a \times \sqrt{2}a \times \sqrt{2}a$ unit cell (a represents a simple perovskite unit) with $P2_1/c$ space group. The unusual high valence state of Fe^{4+} in Ca_2FeMnO_6 is clearly indicated by the single component with a small isomer shift (IS) value of 0.02 mm/s in the Mössbauer spectrum at room temperature (Figure 2a). Interestingly, the compound was found to show CD at low temperatures.

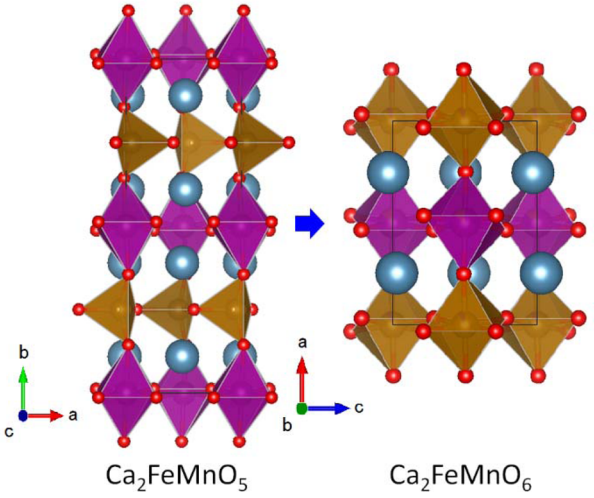

Figure 1. Crystal structure of the layered double perovskite Ca_2FeMnO_6 (right) obtained by topochemical oxidation of the brownmillerite $CaFe_2MnO_5$ (left) at a low temperature. Blue, brown, purple, and red spheres represent Ca, Fe, Mn, and O ions, respectively.

As described above, charge-disproportionated Fe^{3+} and Fe^{5+} ions in the perovskite $CaFeO_3$ and in the *A*-site-ordered double perovskite $CaCu_3Fe_4O_{12}$ are ordered in a rock-salt type manner, making a three-dimensional alternating arrangement of large $Fe^{3+}O_6$ and small $Fe^{5+}O_6$ octahedra. The alternating redistribution of the ligand holes ($2d^5\underline{L} \rightarrow d^5 + d^5\underline{L}^2$) makes the Fe−O bonds alternately shorter and longer than the average in the three-dimensional network.[5,18] This raises the question of what kind of ordered arrangement of the charge-disproportionated Fe^{3+} and Fe^{5+} ions is stabilized in Ca_2FeMnO_6 with the two-dimensional layers of Fe^{4+}. While the Ruddlesden−Popper-type layered oxide $Sr_2Fe^{4+}O_4$ does not show CD, $Sr_3Fe_2O_7$, which consists of double layers of $Fe^{4+}O_6$ octahedra, shows strong evidence for CD.[19] The CD structure in $Sr_3Fe_2O_7$ is expected to have a rock-salt-like alternating arrangement of large $Fe^{3+}O_6$ and small $Fe^{5+}O_6$ octahedra within the double layer, although the CD pattern was not clarified. Thus, CD in the isolated single layer of the $Fe^{4+}O_6$ octahedra makes this newly discovered layered perovskite Ca_2FeMnO_6 unique.

In this paper, we report our investigation of the CD and magnetic transitions in Ca_2FeMnO_6. We describe our detailed analysis of neutron and synchrotron X-ray powder diffraction data revealing the ordered arrangement of the charge-disproportionated Fe^{3+} and Fe^{5+} ions and an unusual noncollinear magnetic structure. We also discuss the CD and magnetic transition behaviors.

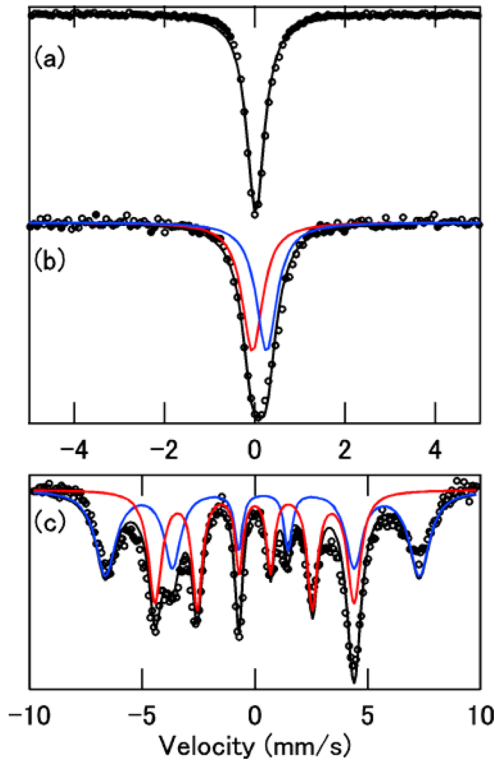

Figure 2. Mössbauer spectra of Ca_2FeMnO_6 at (a) room temperature, (b)150 K, and (c) 6 K. The dots are observed experimental data. The spectrum at room temperature is fitted with Fe^{4+}, and those at low temperatures are fitted with Fe^{3+} (blue) and Fe^{5+} (red). The spectrum at 6 K consists of magnetically ordered sextets of Fe^{3+} and Fe^{5+}, indicating the sample is in a magnetically ordered state.

EXPERIMENTAL SECTION

A polycrystalline sample of Ca_2FeMnO_6 was obtained by oxidizing the brownmillerite Ca_2FeMnO_5[20,21] topochemically with ozone at 200 °C as described in a previous report.[17] Details of the synthesis and the crystal structure at room temperature are given in Supporting Information. The crystal and magnetic structures at low temperatures (2−300 K) were refined by synchrotron X-ray diffraction (SXRD) and neutron diffraction (ND). The sample was packed into a glass capillary that was rotated during the SXRD measurement at beamline BL02B2 in SPring-8, Japan. The diffraction data produced at a wavelength 0.775 Å were analyzed by the Rietveld method using the program RIETAN-FP.[22] The ND experiments with the time-of-flight method for about 2.0 g of sample were performed at beamline WISH of ISIS at RAL, U.K. The data were analyzed with the FullProf program.[23]

Magnetic properties were measured with a commercial Quantum Design MPMS SQUID magnetometer. Temperature dependence of the magnetic susceptibility was measured at 5−300 K in an external magnetic field of 10 kOe. Field dependence of the magnetization was determined by measurements under fields ranging from −50 to 50 kOe. The ^{57}Fe Mössbauer spectra were also observed in transmission geometry in combination with a constant-acceleration spectrometer using ^{57}Co/Rh as a radiation source. α-Fe was used as a control for velocity calibration and isomer shift. The obtained spectra were fitted by a least-squares method with Lorentzian functions.

RESULTS AND DISCUSSION

On cooling, a structural transition due to CD was observed in the ND patterns. Looking at the ND patterns in detail, we notice a small but definite increase in the diffraction intensity at

DOI: 10.1021/jacs.5b03712
J. Am. Chem. Soc. 2015, 137, 7468−7473

d = 5.3 Å below 200 K (inset of Figure 3). This peak can be indexed as 010 and 001 of the $2a \times \sqrt{2}a \times \sqrt{2}a$ unit cell. Note

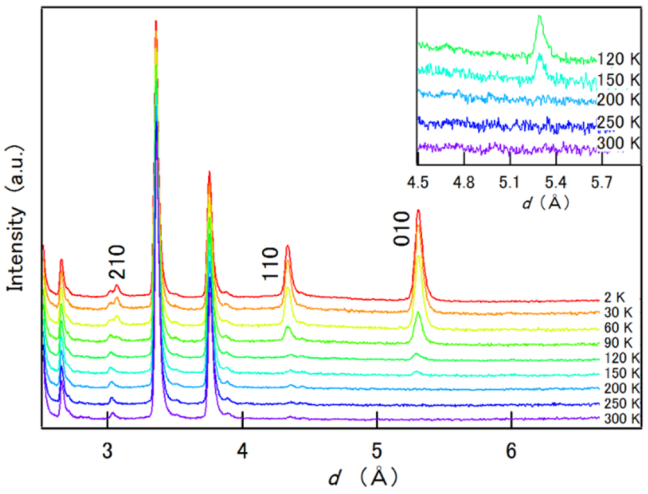

Figure 3. Neutron diffraction patterns of Ca_2FeMnO_6 measured between 300 and 2 K. The 010, 110, and 210 peaks are magnetic reflections observed below 95 K. Inset shows an expanded view of the diffraction patterns from 300 to 120 K around d = 5.3 Å.

that, as will be explained later, the evolution of this ND peak was not due to the magnetic transition. A corresponding change in the SXRD patterns at the same diffraction position is not evident. Since neutron diffraction is much more sensitive to oxygen displacements than X-ray diffraction, the transition seems to be mainly associated with small shifts of oxygen atoms. The 010 and 001 ND peaks are indicative of a superstructure modulation along the [110] direction of the simple perovskite structure. When the oxygen atoms in the FeO_6 octahedral layers shift to make long and short Fe−O bonds alternately, a checkerboard arrangement of the two distinct FeO_6 octahedra in the two-dimensional layers gives a superstructure modulation along the [110] direction. Because the Fe^{3+}−O bonds are longer than the Fe^{5+}−O bonds, the development of this superstructure ND peak strongly indicates that CD occurs in the FeO_6 layers at the temperature below 200 K. The checkerboard-type Fe site CD model in the layered double perovskite allows a $2a \times \sqrt{2}a \times \sqrt{2}a$ unit-cell crystal structure with the $P\bar{1}$ symmetry, but the observed ND intensity from the superstructure was too weak to refine the modulated structure precisely.

The Mössbauer spectrum obtained at 150 K (Figure 2b) also shows CD from Fe^{4+} at high-temperature to Fe^{3+} and Fe^{5+} below 200 K. It is broader than the spectrum obtained at room temperature and cannot be fitted with a single component. It is reproduced well by two singlet components with almost equal intensities (47.6% and 52.4%). Their ISs are 0.28 and −0.05 mm/s, which are typical for Fe^{3+} and Fe^{5+}, respectively.[8] We therefore conclude that Fe^{4+} in Ca_2FeMnO_6 shows CD below 200 K and that the charge-disproportionated Fe^{3+} and Fe^{5+} are ordered in a checkerboard-type manner in the two-dimensional layers. Importantly, this CD transition is not accompanied by the magnetic transition, and thus the high-temperature paramagnetic Fe^{4+} changes to paramagnetic Fe^{3+} and Fe^{5+} at the CD transition temperature. It should be pointed out that in the temperature dependence of resistivity, no anomaly is seen at the CD transition temperature. The resistivity at room temperature is about 3.8 Ω·cm and increases with decreasing temperature (Figure SI 3, Supporting Information). This semiconducting behavior is in sharp contrast to the metal-to-insulator transitions seen at the CD transition temperatures in $CaFeO_3$ and $CaCu_3Fe_4O_{12}$, and may reflect the three-dimensional nature of these materials in contrast to the layered structure of Ca_2FeMnO_6.

Figure 4 shows the temperature dependence of magnetic susceptibility. The observed magnetic susceptibility cannot be

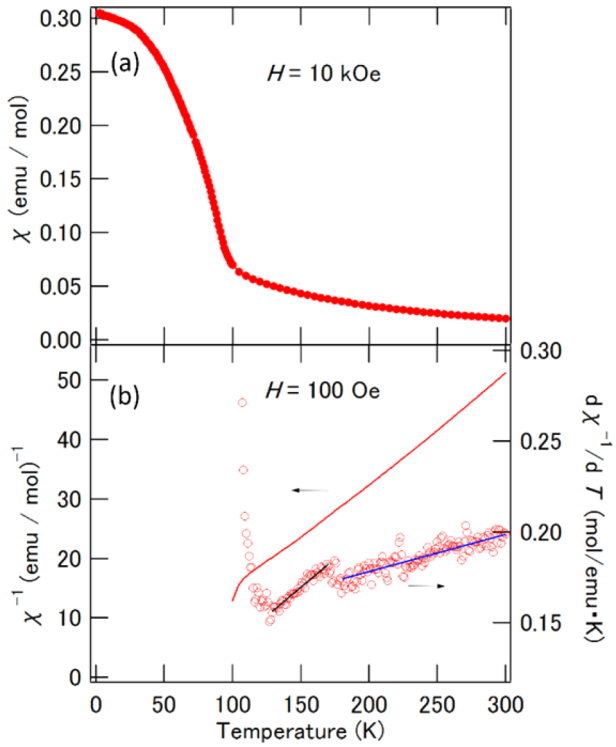

Figure 4. Temperature dependence of (a) the magnetic susceptibility measured under 10 kOe and (b) the inverse susceptibility in 100 Oe and its derivative. The lines in the derivative are guides for eyes.

fitted to a single Curie−Weiss law. A change of inverse susceptibility slope can be seen around 180 K as we clearly see in the temperature dependence of the derivative (Figure 4b), which can indicate the CD transition at this temperature. The temperature we see the anomaly is close to the CD transition temperature suggested by NPD and Mössbauer results. A magnetic transition occurs at about 95 K, where a discontinuity of the magnetization is clearly observed. Note that this magnetic transition temperature is much lower than the CD transition temperature. The development of a few ND peaks like 010, 110, and 210 is clearly evident below the magnetic transition temperature, suggesting that those diffraction peaks are due to magnetic order (Figure 3). The results are also consistent with the previously reported Mössbauer spectroscopy result at 5 K, where two magnetically ordered sextet components were observed (Figure 2c). The IS of each spectrum component is 0.35 or −0.01 mm/s and the hyperfine field is 43.4 or 27.4 T, which are typical values for Fe^{3+} or Fe^{5+}, respectively. In Ca_2FeMnO_6, therefore, the charge-disproportionated Fe^{3+} and Fe^{5+}, which are checkerboard-type arranged in the two-dimensional layers, are magnetically ordered below 95 K. The observed behavior (that with decreasing temperature the magnetic transition follows the CD transition) is similar to that observed in $CaFeO_3$ (T_{CD} = 290 K and T_{mag} = 115 K)[7] but

DOI: 10.1021/jacs.5b03712
J. Am. Chem. Soc. 2015, 137, 7468−7473

Table 1. Refined Crystal and Magnetic Structure Parameters Obtained from ND Data for Ca_2FeMnO_6 at 2 K[a]

(a) Crystal Structure[b]				
atom	x	y	z	B (Å^2)
Ca	0.2539(8)	0.503(2)	0.531(2)	0.8(1)
Fe	0.0	0.0	0.0	0.7(1)
Mn	0.5	0.5	0.0	0.9(4)
O1	0.2493(7)	0.062(1)	0.492(1)	0.7(1)
O2	0.033(1)	0.711(2)	0.287(2)	1.6(2)
O3	0.536(1)	0.286(2)	0.715(2)	1.2(2)
(b) Magnetic Structure				
spin	x	y	z	moment (μ_B)
Fe^{3+} at (0.0, 0.5, 0.0)	2.47(4)	−1.6(2)	−1.6(2)	3.32(5)
Fe^{5+} at (0.0, 0.0, 0.5)	−1.48(3)	0.9(1)	0.9(1)	1.99(3)
Mn^{4+} at (0.5, 0.5, 0.0)	1.48(3)	0.9(1)	0.9(1)	1.99(3)
Mn^{4+} at (0.5, 0.0, 0.5)	−1.48(3)	−0.9(1)	−0.9(1)	1.99(3)

[a] R_{WP} = 5.46%. [b] Space group: $P2_1/c$, a = 7.4951(4) Å, b = 5.2960(2) Å, c = 5.3174(3) Å, and β = 89.99(1)°. Small amounts of antisite occupations at the Fe and Mn sites, 7.2(4)% and 14.6(2)%, respectively, were included in the refinement.

differs from that of the simultaneous CD and magnetic transitions seen in the A-site-ordered perovskite $CaCu_3Fe_4O_{12}$ ($T_{CD} = T_{mag}$ = 210 K).[18]

The ground state magnetic structure of Ca_2FeMnO_6 was analyzed with the ND data collected at 2 K. The observed diffraction pattern is well reproduced by contributions from both the layered double-perovskite crystal structure and the magnetic structure of the Fe^{3+}, Fe^{5+}, and Mn^{4+} spins. Because the number of major ND peaks due to charge-disproportionated structural modulation (d = 5.3 Å) and magnetic ordering (for example, d = 3.1, 4.3, and 5.3 Å) is small, unconstrained analysis of the detailed crystal and magnetic structures is not feasible. SXRD below both the CD and magnetic transition temperatures is quite similar to that obtained at room temperature, suggesting that the structural modulation due to CD is not so significant. We thus refine the layered double-perovskite crystal structure with the $2a \times \sqrt{2}a \times \sqrt{2}a$ unit-cell ($P2_1/c$) but the magnetic moments at the Fe and Mn sites are treated with $P\bar{1}$ symmetry creating two inequivalent Fe (and Mn) sites in a checkerboard arrangement. We also constrain the magnetic moments of Fe^{3+}, Fe^{5+}, and Mn^{4+} in a ratio of 5:3:3 according to their nominal values.

Attempts to refine the magnetic structure with possible collinear spin arrangement models were not successful, and the observed magnetic ND peak intensities could not be reproduced. Noncollinear spin structure models were then introduced, and the final refinement result (Table 1), which reproduces the observed diffraction pattern well, is shown in Figure 5. The noncollinear spin structure model obtained is illustrated in Figure 6. Because no other arrangement of the magnetic moments reproduces the observed magnetic intensities well, the result also confirms the checkerboard-type arrangement of Fe^{3+} and Fe^{5+}. All spins are on the (0 1 1) plane and tilted 41.8° from the a axis. The spin direction is close to one along the [111] axis of the unit cell. The neighboring Mn^{4+} spins in the MnO_6 octahedral layers couple antiferromagnetically, so the Mn-spin sublattice does not produce net magnetization. The Fe^{3+} and Fe^{5+} spins in the FeO_6 octahedral layers also couple antiferromagnetically, producing a net ferrimagnetic order. For the interlayer magnetic coupling, each Fe^{3+} or Fe^{5+} spin makes an angle of 83.5° with the nearest Mn spin. Because a $4a$ magnetic superstructure peak ($d \approx 15$ Å) was not evident in the observed

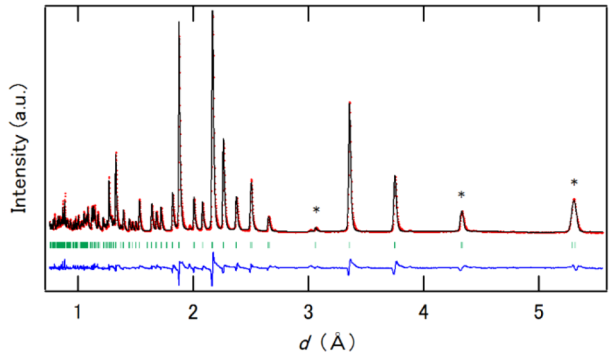

Figure 5. Result of the Rietveld refinement of the neutron diffraction data for Ca_2FeMnO_6 at 2 K. The dots and solid line represent observed and calculated patterns, respectively. The plot below the diffraction patterns is the difference between the observed and calculated intensities. Vertical marks below the profiles are Bragg reflection positions. Marked peaks with an asterisk are typical magnetic reflections.

ND pattern, checkerboard-type CD layers align in an "in phase" manner along the stacking direction; i.e., the cations align Fe^{3+}-Mn^{4+}-Fe^{3+} and Fe^{5+}-Mn^{4+}-Fe^{5+} along the [100] axis.

The refined magnetic moments of Fe^{3+} (S = 5/2), Fe^{5+} (S = 3/2), and Mn^{4+} (S = 3/2) are, respectively, 3.36(5), 2.02(3), and 2.02(3) μ_B, which are reasonably consistent with but slightly smaller than the values expected from their valences due to covalency effects or a small amount of antisite occupations at the B site. The spontaneous magnetization (along the [1 −1 −1] direction) calculated from the refined moments in the ferrimagnetic spin structure is 0.67 μ_B/f.u., which agrees well with the value observed at 5 K of 0.5 μ_B/f.u. (Figure 7).

From the results of the crystal and magnetic structure analyses described above, we can deduce that the most probable arrangement of Fe ion in the charge-disproportionated Ca_2FeMnO_6 is a checkerboard-type arrangement of Fe^{3+} and Fe^{5+} within the FeO_6 octahedral layers and that there is in-phase stacking of the charge states. The magnetic structure in Ca_2FeMnO_6 is very different from those of the related perovskite-structure oxides like $CaFeO_3$ and $SrFeO_3$, in which helical magnetic structures are stabilized,[10,24−28] and $CaMnO_3$, in which the G-type antiferromagnetic structure is stabilized.[29]

DOI: 10.1021/jacs.5b03712
J. Am. Chem. Soc. 2015, 137, 7468−7473

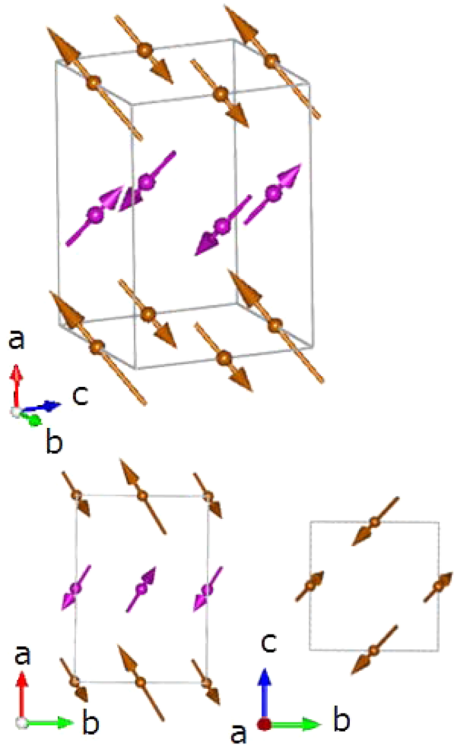

Figure 6. Noncollinear magnetic structure of charge-disproportionated Ca_2FeMnO_6. The Fe^{3+} and Fe^{5+} spins (brown) couple antiferromagnetically in the FeO_6 octahedral layers, producing the ferrimagnetism. The Mn^{4+} spins (purple) are also ordered antiferromagnetically in the MnO_6 octahedral layers.

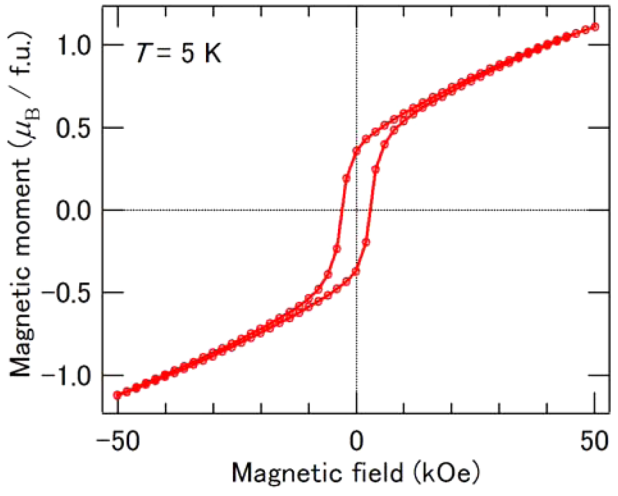

Figure 7. *M* (magnetic moment)-*H* (field) behavior of Ca_2FeMnO_6 at 5 K.

The nearest-neighbor magnetic interactions in Ca_2FeMnO_6 arise from near-linear $Fe^{3+}(d^5)-O-Fe^{5+}(d^3)$, $Fe^{3+}(d^5)-O-Mn^{4+}(d^3)$, $Fe^{5+}(d^3)-O-Mn^{4+}(d^3)$, and $Mn^{4+}(d^3)-O-Mn^{4+}(d^3)$ superexchange paths. According to the Kanamori–Goodenough rules, 180° d^3-O-d^3 gives weak antiferromagnetic interaction while d^5-O-d^3 gives moderate ferromagnetic interaction.[30−32] This classical rule predicts a collinear magnetic structure where the Mn^{4+} spins are antiferromagnetically ordered in the MnO_6 layers, while the Fe^{3+} and Fe^{5+} spins in the FeO_6 layers are ferromagnetically ordered and the interlayer $Fe^{3+}-Mn^{4+}$ and $Fe^{5+}-Mn^{4+}$ are ordered ferromagnetically and antiferromagnetically, respectively. The observed magnetic structure, however, apparently differs from the predicted one, suggesting that in Ca_2FeMnO_6 more complicated interactions play important roles in the magnetism. It is interesting to note here that the charge disproportionation can be described as the two-dimensional localization of ligand holes with effective spins. As seen in the helical magnetic structure in $CaFeO_3$, the ligand hole spins can mediate longer-range magnetic interactions than the nearest-neighbor one. Although the d^3 ($S = 3/2$) spins in the MnO_6 octahedral layers are ordered antiferomagnetically like those in $CaMnO_3$, the ligand hole spins modulate the interlayer magnetic coupling, leading to the noncollinear magnetic structure. The magnetic transition temperature in Ca_2FeMnO_6 is also comparable with the magnetic transition temperature of $CaFeO_3$ (~115 K), suggesting that the essential magnetism arises from the interactions involving the effective spins of ligand holes. Therefore, the localization of the ligand holes in the two-dimensional layers plays an important role in the unique noncollinear magnetic structure of Ca_2FeMnO_6.

CONCLUSIONS

We have investigated the CD and magnetic transition behaviors in the newly discovered layered double-perovskite Ca_2FeMnO_6 with a two-dimensional arrangement containing high valence Fe^{4+} at room temperature. With decreasing temperature, the CD transition from Fe^{4+} to Fe^{3+} and Fe^{5+} takes place around 200 K and magnetic transition occurs at 95 K, far below the CD transition temperature. Detailed analysis of the low-temperature ND patterns revealed that below 95 K the charge-disproportionated Fe^{3+} and Fe^{5+} are ordered in a checkerboard pattern in the two-dimensional FeO_6 octahedral layers and the checkerboard-type layers stack in an in-phase manner. The ground state magnetic structure is a commensurate but noncollinear one, where the neighboring spins in the FeO_6 and MnO_6 octahedral layers couple antiferromagnetically with the interlayer tilts of 83.5° between the Fe and Mn spins. This magnetic structure produces the ferrimagnetic moment in the FeO_6 octahedral layers, and the refined moment, 0.67 μ_B/f.u. along the [1 −1 −1] direction, from the ND analysis agrees well with the spontaneous magnetization observed in the magnetization measurement (0.5 μ_B/f.u. at 5 K). Two-dimensional localization of the ligand holes with effective spins plays an important role in the noncollinear magnetic structure of Ca_2FeMnO_6.

ASSOCIATED CONTENT

Supporting Information

Results of the Rietveld refinement of neutron diffraction data at room temperature and the resistivity measurement for Ca_2FeMnO_6. The Supporting Information is available free of charge on the ACS Publications website at DOI: 10.1021/jacs.5b03712.

AUTHOR INFORMATION

Corresponding Author

*shimak@scl.kyoto-u.ac.jp

Notes

The authors declare no competing financial interest.

ACKNOWLEDGMENTS

We thank D. Kan, K. Hirai, and H. Seki in ICR, Kyoto University, Japan for useful discussion. The synchrotron

DOI: 10.1021/jacs.5b03712
J. Am. Chem. Soc. 2015, 137, 7468−7473

radiation experiments at SPring-8 were performed with the approval of the Japan Synchrotron Radiation Research Institute (proposal Nos: 2013B1226 and 2014B1770). This work was supported by Grants-in-Aid for Scientific Research (Nos. 22740227 and 24540346), by a grant for the Joint Project of Chemical Synthesis Core Research Institutions from MEXT, and by a JST-CREST program of Japan. Support was also provided by EPSRC, STFC and the Royal Society, U.K..

REFERENCES

(1) Kanamaru, F.; Miyamoto, H.; Mimura, Y.; Koizumi, M.; Shimada, M.; Kume, S.; Shin, S. *Mater. Res. Bull.* **1970**, *5*, 257.
(2) Gallagher, P. K.; MacChesney, J. B.; Buchanan, D. N. E. *J. Chem. Phys.* **1964**, *41*, 2429.
(3) Hayashi, N.; Yamamoto, T.; Kageyama, H.; Nishi, M.; Watanabe, Y.; Kawakami, T.; Matsushita, Y.; Fujimori, A.; Takano, M. *Angew. Chem., Int. Ed.* **2011**, *50*, 12547.
(4) Zaanen, J.; Sawatzky, G. A.; Allen, J. W. *Phys. Rev. Lett.* **1985**, *55*, 418.
(5) Bocquet, A. E.; Fujimori, A.; Mizokawa, T.; Saitoh, T.; Namatame, H.; Suga, S.; Kimizuka, N.; Takeda, Y.; Takano, M. *Phys. Rev. B* **1992**, *45*, 1561.
(6) Kawasaki, S.; Takano, M.; Kanno, R.; Takeda, T.; Fujimori, A. *J. Phys. Soc. Jpn.* **1998**, *67*, 1529.
(7) Takeda, T.; Kanno, R.; Kawamoto, Y.; Takano, M.; Kawasaki, S.; Kamiyama, T.; Izumi, F. *Solid State Sci.* **2000**, *2*, 673.
(8) Takano, M.; Nakanishi, N.; Takeda, Y.; Naka, S.; Takada, T. *Mater. Res. Bull.* **1977**, *12*, 923.
(9) Takeda, Y.; Naka, S.; Takano, M.; Shinjo, T.; Takada, T.; Shimada, M. *Mater. Res. Bull.* **1978**, *13*, 61.
(10) Woodward, P. M.; Cox, D. E.; Moshopoulou, E.; Sleight, A. W.; Morimoto, S. *Phys. Rev. B* **2000**, *62*, 844.
(11) Morimoto, S.; Yamanaka, T.; Tanaka, M. *Physica B* **1997**, *237*−*238*, 66.
(12) Yamada, I.; Takata, K.; Hayashi, N.; Shinohara, S.; Azuma, M.; Mori, S.; Muranaka, S.; Shimakawa, Y.; Takano, M. *Angew. Chem.* **2008**, *120*, 7140.
(13) Shimakawa, Y.; Takano, M. *Z. Anorg. Allg. Chem.* **2009**, *635*, 1882.
(14) Mizumaki, M.; Chen, W. T.; Saito, T.; Yamada, I.; Attfield, J. P.; Shimakawa, Y. *Phys. Rev. B* **2011**, *84*, 094418.
(15) Shimakawa, Y.; Mizumaki, M. *J. Phys.: Condens. Matter* **2014**, *26*, 473203.
(16) Ganesanpotti, S.; Tassel, C.; Hayashi, N.; Goto, Y.; Bouilly, G.; Yajima, T.; Kobayashi, Y.; Kageyama, H. *Eur. J. Inorg. Chem.* **2014**, *2014*, 2576.
(17) Hosaka, Y.; Ichikawa, N.; Saito, T.; Haruta, M.; Kimoto, K.; Kurata, H.; Shimakawa, Y. *Bull. Chem. Soc. Jpn.* **2015**, in press.
(18) Chen, W.-T.; Saito, T.; Hayashi, N.; Takano, M.; Shimakawa, Y. *Sci. Rep.* **2012**, *2*, 449.
(19) Dann, S. E.; Weller, M. T.; Currie, D. B.; Thomas, M. F.; Al-Rawwas, A. D. *J. Mater. Chem.* **1993**, *3*, 1231.
(20) Nakahara, Y.; Kato, S.; Sugai, M.; Ohshima, Y.; Makino, K. *Mater. Lett.* **1997**, *30*, 163.
(21) Ramezanipour, F.; Cowie, B.; Derakhshan, S.; Greedan, J. E.; Cranswick, L. M. D. *J. Solid State Chem.* **2009**, *182*, 153.
(22) Izumi, F.; Momma, K. *Solid State Phenom.* **2007**, *130*, 15.
(23) Rodríguez-Carvajal, J. *Physica B* **1993**, *192*, 55.
(24) Takeda, T.; Yamaguchi, Y.; Watanabe, H. *J. Phys. Soc. Jpn.* **1972**, *33*, 967.
(25) Oda, H.; Yamaguchi, Y.; Takei, H.; Watanabe, H. *J. Phys. Soc. Jpn.* **1977**, *42*, 101.
(26) Takeda, T.; Komura, S.; Watanabe, N. *Proc. Int. Conf. Ferrites (ICF-9)* **1980**, 385.
(27) Nasu, S.; Abe, T.; Yamamoto, K.; Endo, S.; Takano, M.; Takeda, Y. *Hyperfine Interact.* **1991**, *67*, 529.
(28) Mostovoy, M. *Phys. Rev. Lett.* **2005**, *94*, 137205.
(29) Wollan, E. O.; Koehler, W. C. *Phys. Rev.* **1955**, *100*, 545.
(30) Goodenough, J. B. *J. Phys. Chem. Solids* **1958**, *6*, 287.
(31) Kanamori, J. *J. Phys. Chem. Solids* **1959**, *10*, 87.
(32) Goodenough, J. B. *Magnetism and the Chemical Bond*; Interscience Publishers, John Wiley & Sons: New York, London, 1963.

DOI: 10.1021/jacs.5b03712
J. Am. Chem. Soc. 2015, 137, 7468−7473